



IR-to-visible image upconverter under nonlinear crystal thermal gradient operation

H. MAESTRE,* A. J. TORREGROSA, C. R. FERNÁNDEZ-POUSA, AND J. CAPMANY

Department of Communications Engineering, Universidad Miguel Hernández, Avda.de la Universidad s/n 03202 Elche (Alicante), Spain

*hmaestre@umh.es

Abstract: In this work we study the enhancement of the field-of-view of an infrared image up-converter by means of a thermal gradient in a PPLN crystal. Our work focuses on compact upconverters, in which both a short PPLN crystal length and high numerical aperture lenses are employed. We found a qualitative increase in both wavelength and angular tolerances, compared to a constant temperature upconverter, which makes it necessary a correct IR wavelength allocation in order to effectively increase the up-converted area.

© 2018 Optical Society of America under the terms of the [OSA Open Access Publishing Agreement](#)

OCIS codes: (190.4223) Nonlinear wave mixing; (110.3080) Infrared imaging; (140.3613) Lasers, upconversion; (190.7220) Upconversion.

References and links

1. J. S. Dam, P. Tidemand-Lichtenberg, and C. Pedersen, "Room-temperature mid-infrared single-photon spectral imaging," *Nat. Photonics* **6**(11), 788–793 (2012).
2. S. Fan, F. Qi, T. Notake, K. Nawata, Y. Takida, T. Matsukawa, and H. Minamide, "Diffraction-limited real-time terahertz imaging by optical frequency up-conversion in a DAST crystal," *Opt. Express* **23**(6), 7611–7618 (2015).
3. C. Pedersen, Q. Hu, L. Høgstedt, P. Tidemand-Lichtenberg, and J. S. Dam, "Non-collinear upconversion of infrared light," *Opt. Express* **22**(23), 28027–28036 (2014).
4. H. Maestre, A. J. Torregrosa, and J. Capmany, "IR Image upconversion using band-limited ASE illumination fiber sources," *Opt. Express* **24**(8), 8581–8593 (2016).
5. H. Maestre, A. J. Torregrosa, and J. Capmany, "IR Image Upconversion Under Dual-Wavelength Laser Illumination," *IEEE Photonics J.* **8**(6), 1–8 (2016).
6. K. Regelskis, J. Želudevičius, N. Gavrilin, and G. Račiukaitis, "Efficient second-harmonic generation of a broadband radiation by control of the temperature distribution along a nonlinear crystal," *Opt. Express* **20**(27), 28544–28556 (2012).
7. Y. L. Lee, Y.-C. Noh, C. Jung, T. Yu, D.-K. Ko, and J. Lee, "Broadening of the second-harmonic phase-matching bandwidth in a temperature-gradient-controlled periodically poled Ti:LiNbO₃ channel waveguide," *Opt. Express* **11**(22), 2813–2819 (2003).
8. Y. L. Lee, B. A. Yu, C. Jung, Y. C. Noh, J. Lee, and D. K. Ko, "All-optical wavelength conversion and tuning by the cascaded sum- and difference frequency generation (cSFG/DFG) in a temperature gradient controlled Ti:PPLN channel waveguide," *Opt. Express* **13**(8), 2988–2993 (2005).
9. J. Chang, Z. Yang, and Q. Sun, "Broadband mid-infrared difference frequency generation in uniform grating periodically poled lithium niobate," *Optik (Stuttg.)* **126**(11–12), 1123–1127 (2015).
10. H. J. Maestre Vicente, A. J. Torregrosa, and J. Capmany, "Application of a temperature-gradient PPLN crystal for IR image up-conversion," in *Conference on Lasers and Electro-Optics*, OSA Technical Digest (Optical Society of America, 2016), paper JTU5A.61.
11. L. Høgstedt, A. Fix, M. Wirth, C. Pedersen, and P. Tidemand-Lichtenberg, "Upconversion-based lidar measurements of atmospheric CO₂," *Opt. Express* **24**(5), 5152–5161 (2016).
12. J. Capmany, A. J. Torregrosa, H. Maestre, and M. L. Rico, "Miniaturized intra-cavity image up-conversion system based in a 1342 nm YVO₄:Nd³⁺ laser using Type-II phase matching in a bulk KTP crystal combined with a polarizing beam splitter," in *2017 European Conference on Lasers and Electro-Optics - European Quantum Electronics Conference*, (Optical Society of America, 2017), paper CD-14.5 THU.
13. P. Malara, P. Maddaloni, G. Mincuzzi, S. De Nicola, and P. De Natale, "Non-collinear quasi phase matching and annular profiles in difference frequency generation with focused Gaussian beams," *Opt. Express* **16**(11), 8056–8066 (2008).
14. M. M. Fejer, G. A. Magel, D. H. Jundt, and R. L. Byer, "Quasi-phase-matched second harmonic generation: tuning and tolerances," *IEEE J. Quantum Electron.* **28**(11), 2631–2654 (1992).
15. R. A. Haas, "Influence of a constant temperature gradient on the spectral-bandwidth of second-harmonic generation in nonlinear crystals," *Opt. Commun.* **113**(4–6), 523–529 (1995).

1. Introduction

Image frequency up-conversion in a nonlinear (NL) optical crystal is being investigated in recent years as an attractive alternative to image objects illuminated with (or radiating at) wavelengths in the infrared (IR) by wavelength shift to the visible and near-IR spectral regions. Wavelength shift is accomplished through a sum-frequency mixing (SFM) process in a periodically-poled lithium niobate crystal (PPLN). This technique enables the acquisition of real-time and full unscanned 2D images. It also allows for taking advantage of the better characteristics of image sensors in the visible in terms of noise, speed, resolution, or uncooled operation as compared to existing imaging sensors in different spectral ranges of the infrared and in the THz region [1,2]. An important parameter of an image upconverter is the field-of-view for the incoming IR radiation to be upconverted (or, equivalently, the area of the IR image that will be upconverted). For the full upconversion of the IR illuminated area, the field-of-view of the upconverter has to be approximately equal to or wider than the angular IR incoming spectrum.

Additionally, the field-of-view of the image upconverter is tightly bound to the wavelength spectral content of the IR radiation to be up-converted [3]. Thus, a 2-D image up-conversion requires the participation of a set of different incoming angles in a non-collinear quasi-phase-matching (NCQPM) process. Therefore, a multiple-wavelength illumination source is needed in order to up-convert as many IR incoming angles as possible. In previous works [4, 5] it was shown that broadband or multi-wavelength sources, under proper spectral shaping, can yield a smooth and widened field-of-view in an image upconverter. In contrast, the application of a thermal gradient between the edges of the PPLN crystal induces a variation of the refractive index, and thus a wave-vector mismatch, along the propagation direction, which contributes to broaden the QPM bandwidth even under single-wavelength illumination. This change of the wave-vector mismatch is also a characteristic of chirped PPLN gratings and, therefore, both techniques can be regarded, to some extent, as equivalent. In particular, a thermal gradient allows for reconfiguration of the nonlinear process in the crystal.

Thermal gradient applied to a PPLN crystal has been mainly proposed in the past years as a tool for increasing the number of accepted wavelengths in frequency conversion processes of mode-locked lasers [6] and in broadband generation of near-IR and mid-IR wavelengths [7–9]. Here we explore how the application of a thermal gradient to a PPLN crystal contributes to broaden the angular acceptance of the up-converter in order to increase the up-converted field-of-view while using a single-wavelength laser illumination. Broadband, spectrally shaped illumination sources show reduced brightness, if compared to single-wavelength sources. Thus, a single-wavelength illumination source might be preferred for upconversion purposes since it enables further illumination distances (because of its high brightness) and increased spectral efficiency. In [10] we showed image upconversion field-of-view enhancement under IR single-wavelength illumination and thermal gradient operation in a PPLN crystal. Alternatively, in [11], PPLN thermal gradient operation was also proposed for to the upconversion detection of lidar pulses. Furthermore, we have recently proposed a compact upconverter architecture based on a monolithic intracavity design as an enabling technology for the widespread use of image upconverters [12]. Short focal length lenses (with high numerical apertures) are needed for such compact upconverters so as to couple the infrared image to the NL crystal and, therefore, splitting the incoming IR image in a broad set of angles (angular spectrum). It is thus of interest the identification of the upconverter features that enable such an enhancement of the field-of-view in order to accommodate the angular content of the focused IR image to the accepted angles of the upconverter. In Fig. 1 we show a possible configuration for the compact monolithic upconverter.

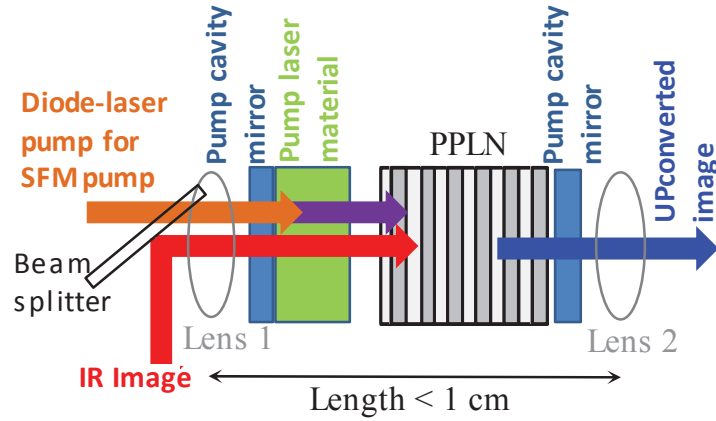


Fig. 1. Schematic of the compact upconverter semimonolithic architecture where short focal length lenses are needed for compactness.

In this work the angular response of the upconverter with a thermal gradient is numerically and experimentally investigated and further insight on the key parameters that play an important role in the angular response widening of the upconverter is provided. Our measurements will show results on the upconversion of images in the SWIR (around 1550 nm) shifted to nearly 631 nm after SFM with a 1064 nm pump wave. Our analysis and conclusions can be readily transferred to the upconversion of additional IR spectral wavelengths.

2. Non-collinear upconversion in a short length PPLN with a thermal gradient

In an image upconverter, the upconverted area (or field-of-view, correspondingly) is a function of the focusing conditions and the nonlinear (NL) crystal angular acceptance. After the incoming IR illumination beam carrying the image spatial information is focused, different parts of the image to be upconverted will correspond to different angles on the NL crystal. Under single-wavelength illumination, the upconversion process restricts to a nearly collinear interaction with a, typically, narrow angular acceptance (narrow field-of-view). Therefore, for the upconversion of wider angles, and thus a wider upconverted area, noncollinear phase-matching (NCPM) must be satisfied. Since NCPM is wavelength sensitive, engineered multiple-wavelength illumination can be used to achieve an effective increase of the NL crystal angular acceptance [4, 5]. The design equation for estimating the angular dependence of the upconverted image, $I_{UP}(\theta)$, as a function of the incoming IR angles θ and under the assumption of a nearly collimated pump wave [Fig. 2(a)] is shown in Eq. (1). $F_{IR}(\theta)$ is the incoming IR angular spectrum (plane-wave decomposition of the IR illumination light after focusing in the NL crystal), $\eta(\theta, \lambda_{IR})$ is the angular upconversion efficiency for every wavelength (λ_{IR}) in the IR illumination spectrum $G_{IR}(\lambda_{IR})$, with most significant wavelengths restricted to the range λ_1 - λ_2 . The number of IR wavelengths, spectral separation and relative intensities can be tailored to provide, after integration, a function which is nearly constant with the incoming angle θ in a targeted angular bandwidth.

$$I_{up}(\theta) \propto F_{IR}(\theta) \int_{\lambda_1}^{\lambda_2} d\lambda_{IR} \cdot \eta(\theta, \lambda_{IR}) \cdot G_{IR}(\lambda_{IR}). \quad (1)$$

Equation (1) is intended for spatially coherent IR illumination sources (i.e. single-mode optical fiber IR sources). More details of the validity of this equation may be found in [4].

Because of the short crystal length in a compact device, the upconversion efficiency is reduced (it scales quadratically with the length of the NL crystal) and thus, an efficient upconversion will rely on high-power IR illumination, which is favored when single-frequency laser sources are selected. Under single-wavelength IR illumination the only way to increase the angular response bandwidth of the upconverter relies on the QPM structure which, after the application of a longitudinal thermal gradient (along z -coordinate, assuming z as the wave propagation axis), yields a widened upconversion angular dependence $\eta'(\theta, \lambda_{IR})$ and, hence, Eq. (1) becomes:

$$I_{up}(\theta) \propto F_{IR}(\theta) \cdot \eta'(\theta, \lambda_{IR}). \quad (2)$$

A thermal gradient across the z -coordinate of the PPLN crystal produces a longitudinal modulation of the refractive index of the interacting waves $n_i(z)$ where $i = IR, pump, up$ stems for IR-illumination, SFM-pump and upconverted waves, respectively. This modulation, in turn, makes the wave-vector mismatch z -dependent as well. Accounting for NCPM (in which, again, the pump-wave is assumed to be a collimated beam) [4, 11, 13], this wave-vector crystal-length dependence can be assessed:

$$\Delta k'(\theta, \lambda, T(z)) = k_{pump} - k_{up} \cos\left(\arcsin\left(\frac{k_{IR}}{k_{up}} \sin(\theta)\right)\right) + k_{IR} \cos(\theta) + \frac{2\pi}{\Lambda}. \quad (3)$$

After second order expansion of trigonometric functions in Eq. (3), we obtain Eq. (4) as:

$$\Delta k'(\theta, \lambda, T(z)) = \Delta k^0 + \frac{k_{IR}}{2} \left(1 - \frac{k_{IR}}{k_{up}}\right) \theta^2. \quad (4)$$

where $k_i = \frac{2\pi}{\lambda_i} n_i(\theta, \lambda_i, T(z))$, Λ is the PPLN grating period and $\Delta k^0 = k_{pump} + k_{IR} - k_{up} + \frac{2\pi}{\Lambda}$.

Small deviations from Λ due to thermal expansion of different PPLN periods at different temperatures can be included and obtained from $\Lambda_n = \Lambda_0 [1 + \alpha(T_n - 25^\circ C) + \beta(T_n - 25^\circ C)^2]$ with Λ_0 the period length at $25^\circ C$, Λ_n the actual period length at temperature T_n for domain n , $\alpha = 1.54 \cdot 10^{-5} \text{ }^\circ C^{-1}$ and $\beta = 5.3 \cdot 10^{-9} \text{ }^\circ C^{-2}$ the thermal expansion coefficients for LiNbO_3 . Therefore, the phase-mismatch $\Delta k'(\theta, z)$ will change at each longitudinal section of the crystal. For fixed interacting wavelengths there is a different IR incoming angle satisfying NCPM for every z -coordinate, thus distinct crystal sections will contribute to enhance different angles in the global angular response [Fig. 2(b)] in contrast to a constant temperature PPLN, where $\Delta k'(\theta)$ is constant with crystal length and hence all crystal sections have the same contribution to the angular response. For a refractive index modulation along the NL crystal, the upconversion efficiency can be calculated as [14,15]:

$$\eta'(\theta, \lambda) \equiv \left| \frac{1}{L} \int_0^{L'} dz e^{\int_0^z -i\Delta k'(\theta, \lambda, T(z)) dz'} \right|^2. \quad (5)$$

where the integral limit $L' = \frac{L}{2 \cos \theta}$ is the z -coordinate projection of the incoming IR rays at different θ [13]. Numerical integration of Eq. (5) is employed for the calculations shown throughout this paper. Alternatively, an analytical solution based on Fresnel integrals can be obtained for Eq. (5) [15], but this solution requires the thermal gradient along the NL crystal to be linear, which does not hold completely in our case. In our experiments, we directly apply heat/cold to the NL crystal edges [Fig. 2(a)], as opposed to other approaches. This will be discussed in a different section of the text.

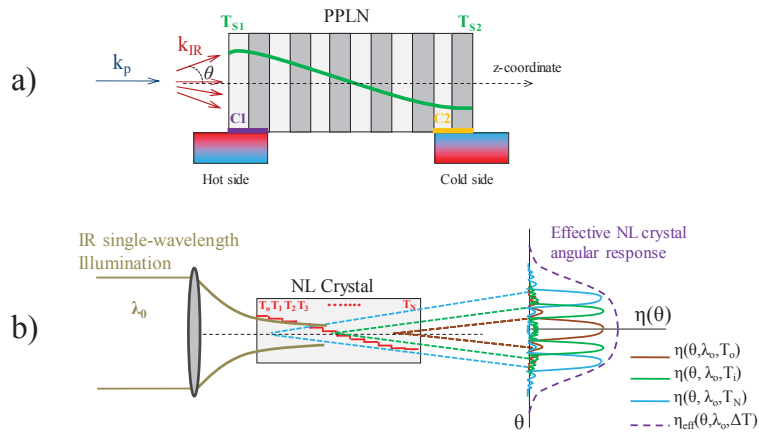


Fig. 2. Coordinate system and important parameters for the thermal gradient PPLN calculations in a). Upconversion of by means of multiple-wavelength illumination under constant temperature operation in b), and conception of different crystal sections providing upconversion at different angles under thermal gradient operation and single-wavelength illumination in c).

Figure 3 represents the condition $\Delta k'(\theta, z) = 0$, that is, the incoming IR angles which are perfectly phase-matched at different crystal positions at a given IR wavelength for different linear temperature gradients and a PPLN period of $\Lambda = 11.785 \mu\text{m}$. When a temperature gradient is set, by allocating the IR wavelength appropriately, the number of favored angles for upconversion can be increased. The amplitude with which each of these angles will contribute to the global upconversion angular response will depend on the accumulated phase (Eq. (5)) that, in turn, depends on the temperature difference $\Delta T = T_{S1} - T_{S2}$, where at the input and output faces of the PPLN [Fig. 2(a)]. This can be seen in [Fig. 3(a)] for a $\Delta T = 20^\circ \text{C}$ and increasing IR illumination wavelengths. In [Fig. 3(b)] we set $\Delta T = 50^\circ \text{C}$ and the same behavior as in [Fig. 3(a)] can be appraised besides an increment of the phase-matched angles.

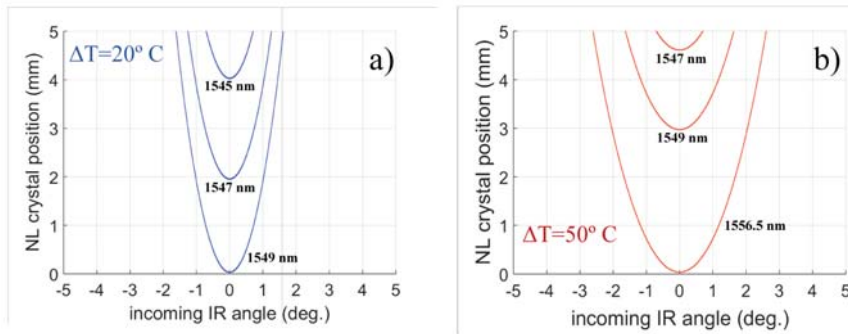


Fig. 3. Representation of the condition $\Delta k'(\theta, z) = 0$ at wavelengths 1545, 1547, and 1549 nm for $\Delta T = 20^\circ \text{C}$ in a) and at wavelengths 1547, 1549 and 1556.5 nm for $\Delta T = 50^\circ \text{C}$ in b).

In order to describe in simple terms the upconversion angular widening using a NL crystal with a thermal gradient under single-wavelength illumination, we recorded the upconversion of a focused IR gaussian beam with a $\lambda_{\text{IR}} = 1551 \text{ nm}$ (Visualization 1), pumped with $\lambda_{\text{pump}} = 1064 \text{ nm}$ and yielding $\lambda_{\text{up}} \approx 631 \text{ nm}$. This IR illumination wavelength is above the NL crystal design wavelength ($\lambda_{\text{QPM}} = 1544.5 \text{ nm}$ at 22°C for our PPLN) and displays a ring-like pattern after the upconversion at room temperature. When the PPLN is heated from 20°C to 60°C the ring-like pattern diameter is reduced and concentrates at the center of the image. When

cooled from 20° C down to 10° C the ring-like pattern diameter grows. It is therefore expected that a temperature gradient, which means the crystal contains a set of different temperatures, will enable the upconversion of a higher number of incoming angles by selecting the temperature limits opportunistically. Consequently, for a given upconverter, which means a given SFM pump wavelength, input focusing lens (i.e. IR angular spectrum) and PPLN grating period, the adequate combination of IR illumination wavelength and thermal gradient may lead to an effective widening of the upconverter field-of-view. It is worth mentioning that this broadening cannot be infinitely widened. At some point, it will show ripples and will be peaked at angles away from $\theta = 0$. From this perspective, a thermal gradient in a PPLN can be exploited to broaden the upconverted images in two different ways. On one hand, it can be used to make $\eta'(\theta, \lambda_{IR})$ as wide as possible, while peaked at $\theta = 0$. This may be of interest in the upconversion of IR beams displaying a nearly ideal (flat-top) low-pass angular spectrum after focusing. On the other hand, it can be used to provide $\eta'(\theta, \lambda_{IR})$ peaked at $|\theta| > 0$ so that the product $F_{IR}(\theta) \cdot \eta'(\theta, \lambda_{IR})$ is effectively widened. This matches the case of our work where the IR illumination spectrum is gaussian, thus showing an angular roll-off which can be compensated after multiplication by a double-peaked $\eta'(\theta, \lambda_{IR})$ function. In the next section we provide numerical calculations on the angular widening of the upconversion process under NL crystal thermal gradient.

3. Thermal gradient influence on IR illumination wavelength allocation

In this section our interest focuses on the normalized upconversion efficiency as a function of the incoming IR illumination angle and wavelength ($\eta'(\theta, \lambda)$). Here, we assess the effect on $\eta'(\theta, \lambda)$ of both the NL crystal temperature difference (ΔT) and the initial/final temperature crystal points when a constant ΔT is maintained. We additionally evaluate the impact of the temperature gradient linearity through the PPLN crystal. These calculations are of interest since they allow optimizing the upconversion angular response and efficiency for a given IR illumination wavelength.

3.1 Influence of initial and final temperature on $\eta'(\theta, \lambda)$

In Fig. 4 we show the effect of changing the temperature difference ($\Delta T = 0, 40, 50$ and 60° C) between the hot side and the cold side of the PPLN crystal.

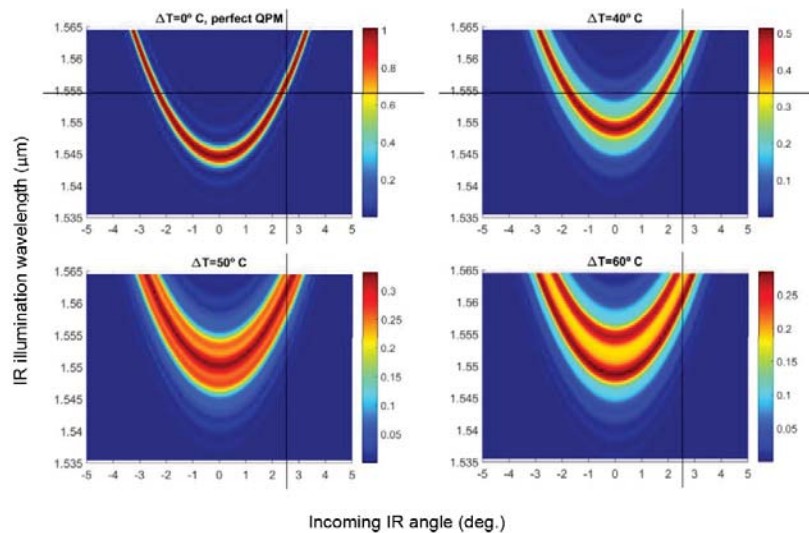


Fig. 4. Numerically obtained upconversion efficiency $\eta'(\theta, \lambda)$ for several NL crystal temperature differences $\Delta T = 0, 40, 50$ and 60° C.

In our calculations we consider a 5 mm length, MgO-doped PPLN crystal with poling period $\Lambda = 11.785 \mu\text{m}$ that maximizes the upconversion at for $\lambda_{\text{IR}} = \lambda_{\text{QPM}} = 1544.5 \text{ nm}$ when pumped with $\lambda_{\text{pump}} = 1064 \text{ nm}$ at room temperature (22°C). The temperature of the cold side remains fixed ($T_{\text{S}2} = 20^\circ \text{C}$) while the temperature of the hot side ($T_{\text{S}1}$) is increased for the different plots of this figure. The case for constant temperature of 22°C throughout the crystal ($\Delta T = 0$) is also included for comparison. In general terms, for a constant temperature in the PPLN, the upconversion efficiency is peaked at $\theta \approx 0$ deg for $\lambda_{\text{IR}} \approx \lambda_{\text{QPM}}$, and it becomes double-peaked at angles $|\theta| > 0$ deg for wavelengths $\lambda_{\text{IR}} > \lambda_{\text{QPM}}$. As it can be seen, when a thermal gradient is applied to the PPLN ($\Delta T > 0$), the upconversion angular response is broadened for long wavelengths but at the expense of efficiency at $\theta \approx 0$, which is distributed to other angles (Fig. 4, colorbars).

Furthermore, this broadening increases as the gradient becomes steeper but the angular response at a given IR wavelength may not yield a smooth profile. Proper wavelength allocation enables both maximizing the widening and reducing the ripple of the angular response. As mentioned earlier, we can either broaden $\eta'(\theta, \lambda_{\text{IR}})$ or the product $F_{\text{IR}}(\theta) \cdot \eta'(\theta, \lambda_{\text{IR}})$. As an example of wavelength allocation, we show the upconversion angular response for $\Delta T = 50^\circ \text{C}$ at $\lambda_{\text{IR}} = 1549 \text{ nm}$ which provided the widest broadening and lowest ripple of the upconverter angular response [Fig. 5(a)]. In [Fig. 5(b)] the IR angular spectrum is taken into consideration. As it can be seen, in this case, the IR illumination wavelength needs to be shifted to $\lambda_{\text{IR}} = 1552 \text{ nm}$ in order to obtain a double-peak angular response that can compensate for the angular roll-off introduced by the incoming angular spectrum. For a given temperature difference, further broadening can be reached by shifting to longer IR illumination wavelengths if a higher degree of ripple of the upconversion angular response can be tolerated. The insets in Fig. 5 show the efficiency angular dependence for the broadened case relative to that for $\Delta T = 0^\circ \text{C}$.

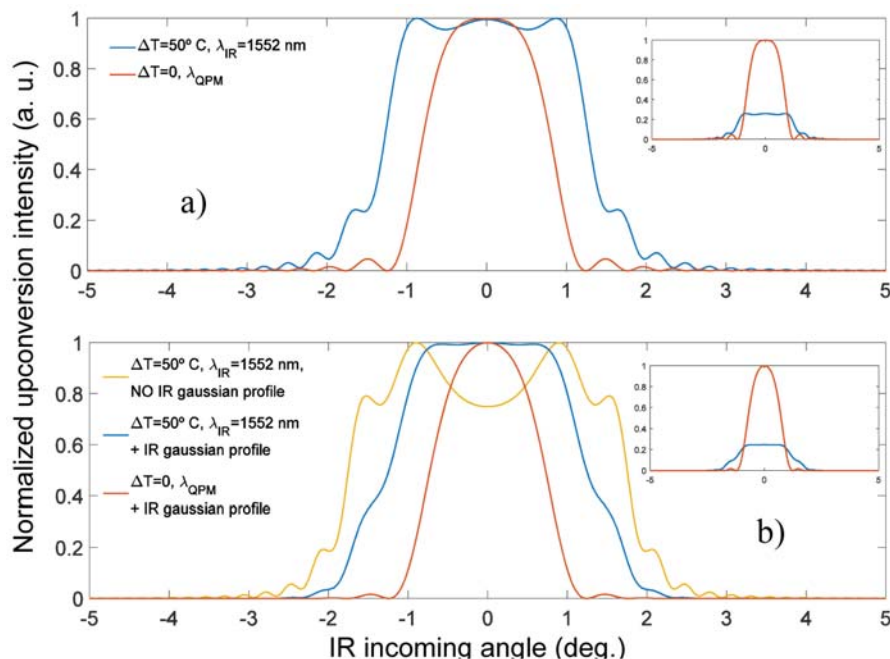


Fig. 5. Upconversion field-of-view broadening optimization for $\Delta T = 50^\circ \text{C}$. In a) $\eta'(\theta, \lambda)$ is optimized for $\lambda_{\text{IR}} = 1549 \text{ nm}$. In b), when the IR incoming angular spectrum is considered, optimized profile takes place at $\lambda_{\text{IR}} = 1552 \text{ nm}$.

We also evaluated the effect of changing PPLN side temperatures, T_{S1} and T_{S2} , while keeping a constant ΔT . In Fig. 6, we plot $\eta'(\theta, \lambda_{IR})$ for several values of T_{S1} and T_{S2} and a fixed temperature difference of $\Delta T = 50^\circ\text{C}$.

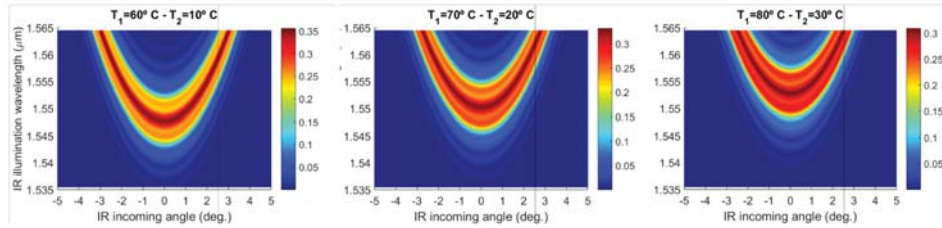


Fig. 6. Effect of different initial and final NL crystal temperature (T_{S1} and T_{S2}) for a fixed $\Delta T = 50^\circ\text{C}$ on the upconversion efficiency $\eta'(\theta, \lambda_{IR})$.

Regardless of a shift to longer wavelengths, the obtained response shows a similar broadening in all three cases. The main difference relies on the ripple or contrast between maxima and minima in the function $\eta'(\theta, \lambda_{IR})$, displaying an angular profile with a different homogeneity at increasing values of both T_{S1} and T_{S2} .

3.2 Thermal gradient linearity

Through evaluation of Eq. (5) and due to the cumulative phase in the integral, it can be noticed that a short-length NL crystal needs a steeper gradient than long-length NL crystals. In addition, after simulation we find that NL crystal edge temperature differences (ΔT) in the range $\Delta T = [20-60]^\circ\text{C}$ are needed to reach an effective upconverted image broadening. Our short-length upconverter will comprise a 5 mm length PPLN crystal. This means that thermal gradients ranging from $40^\circ\text{C}/\text{cm}$ to $120^\circ\text{C}/\text{cm}$ must be achieved along the NL crystal. Generally, the thermal gradient is applied to a few cm NL crystal and accomplished by means of heat flow through a metal sheet with hot/cold sources on its edges where the NL crystal is placed on top of the metal sheet. The gradient is formed across the metal sheet and then transferred to the NL crystal. In our case, this approach would demand a high heatsinking capability on the cold side which is hard to fulfill while maintaining a small footprint of the upconverter. As a consequence of the aforementioned points, we directly attached hot and cold sources near the input and output faces of the PPLN crystal, respectively, so as to force the heat flow through the PPLN crystal.

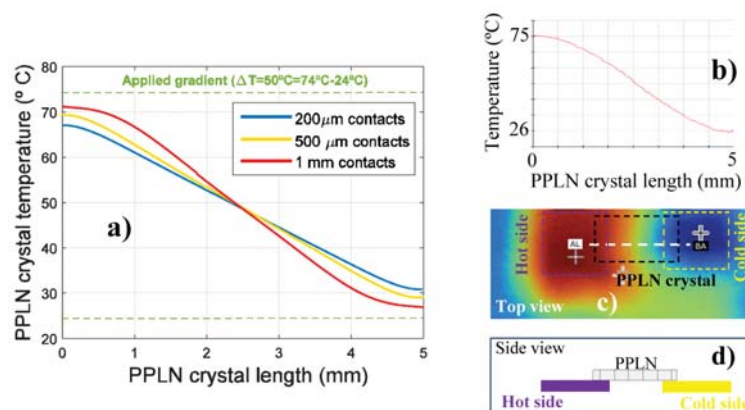


Fig. 7. In a) we show the simulated thermal gradient in the for different contact lengths between the hot/cold sources and the PPLN crystal. In b) it can be seen the measured temperature profile along the NL crystal using a thermal camera. A thermal image of the top view of the thermal gradient setup is plotted in c) and in d) a schematic of the side view.

We performed 3D finite-element method (FEM) for the simulation of thermal distribution in the PPLN under temperature gradient operation. The results are dependent upon the contact area between the hot/cold sources and the PPLN crystal. In [Fig. 7(a)], we plot the calculated longitudinal temperature distribution for different contact areas. Since in our experimental setup the hot and cold sources are wider than the PPLN crystal width (3 mm), the contact width is regarded as 3 mm and the parameter which changes in the simulation is the contact length (C1 and C2 in [Fig. 2(a)]). The shorter the thermal contacts, the more linear is the temperature change in the crystal, but a lower temperature difference is achieved if compared to the applied thermal difference. Longer thermal contacts keep, approximately, the same temperature difference than applied but with a relative nonlinear thermal evolution in the crystal. Although short contacts are better for gradient linearity, we opted (experimentally) for thermal contacts of around 1 mm since extra cooling/heating needed to achieve the desired temperature difference for contacts in the order of 100 μm exceeded our experimental capabilities.

The actual temperature gradient was also measured with a thermal camera and the nonlinear temperature distribution can be noticed in [Fig. 7(b)]. This figure represents the temperature along the white dotted line in [Fig. 7(c)]. In [Fig. 7(c)] we represent the thermal image of the top view of the temperature gradient setup (hot side + PPLN + cold side) where the hot side was heated to 80°C and the cold side was cooled down to 20°C. The hot side (violet dotted line) is a resistive heater and the cold side (yellow dotted line) is a thermoelectric cooler (Peltier element). The schematic side view of the temperature gradient setup is pictured in [Fig. 7(d)].

Thermal gradient deviation from a linear behavior has to be taken into account for predicting the accurate angular response of the upconverter. The differences between linear and nonlinear gradient and the predicted angular response are shown in Fig. 8 for the case $\Delta T = 50^\circ\text{C}$.

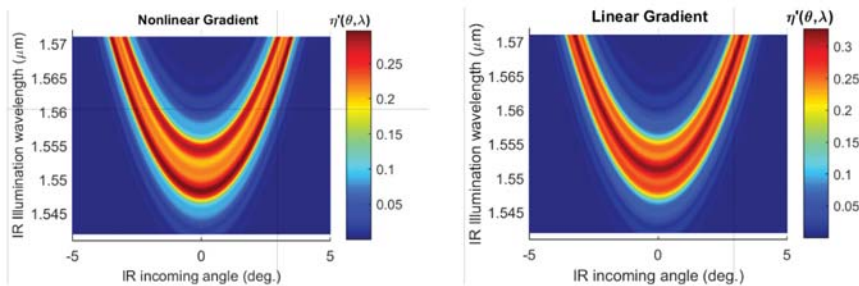


Fig. 8. Comparison between $\eta^*(\theta, \lambda_{IR})$ for the actual (figure on the left) and perfectly linear (figure on the right) thermal gradient for $\Delta T = 50^\circ\text{C}$.

As it can be seen, for a given ΔT the broadening remains similar in both cases but they differ mainly in the angular flatness for every IR wavelength. This has, therefore, to be accounted for in the comparison between measured and calculated upconversion angular dependence data.

4. Experimental results

In this section we present several FOV widening experimental evidences for image upconversion using a temperature gradient PPLN as upconverter. The experimental setup is portrayed in Fig. 9. The upconverter is comprised of a 4-f optical system by means of lenses L1 and L2. The compact temperature gradient PPLN crystal ($\text{MgO}:\text{LiNbO}_3$, 3 mm width, 1mm height, 5 mm length and 11.8 μm poling period) is placed in the focus of the 4-f system. A single-wavelength fiber-coupled tunable laser around 1550 nm is the IR illumination source, which after passing through the target creates a transmission image. The full IR image

is focused in the PPLN by lens L1 (the IR beam width before L1 and its focal lens determine the incoming IR angular spectrum) to a 30 μm diameter spot approximately. An external Nd:YAG laser at 1064 nm acts as the SFM pump wave and is combined with the IR image in the PPLN using a dichroic beam-splitter BS. The pump beam had a power of 40W and was shaped to have a spot diameter of around 1 mm, matching the shortest dimension of the PPLN section. The upconverted image (around 630 nm) is collected by lens L2 and detected and recorded in real-time in a common purpose 8-bit CCD camera. Remaining radiation from pump, IR source and other possible harmonics from the PPLN are eliminated (fully or partially) by the optical filter F. In the following upconversion pictures and visualizations, the bright spot present at the center of the images corresponds to the partially unfiltered second harmonic (532 nm) of the SFG pump wave (1064 nm) which is also generated in the PPLN crystal.

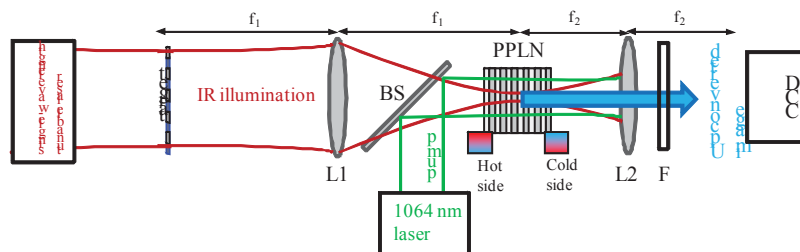


Fig. 9. Experimental setup for the upconversion of IR images under PPLN temperature gradient operation.

In [Visualization 2](#) we recorded real-time (in the clip the time is sped-up x3) how the upconverted area increases while a thermal gradient is applied ($\Delta T = 30^\circ\text{C}$ and $\lambda_{\text{IR}} = 1550\text{ nm}$). We see that before applying the gradient the upconverted profile shows an annular pattern since the IR illumination wavelength is above the design wavelength for perfect QPM at room temperature ($\lambda_{\text{QPM}} = 1544.5\text{ nm}$). When heat is applied to the hot side of the PPLN the whole crystal heats up and $\lambda_{\text{IR}} = 1550\text{ nm}$ becomes perfectly phase-matched hence concentrating the upconversion at $\theta \approx 0$. When the cold side starts cooling, the temperature gradient is achieved, giving rise to a longitudinal phase mismatch thus spreading the upconversion to other angles.

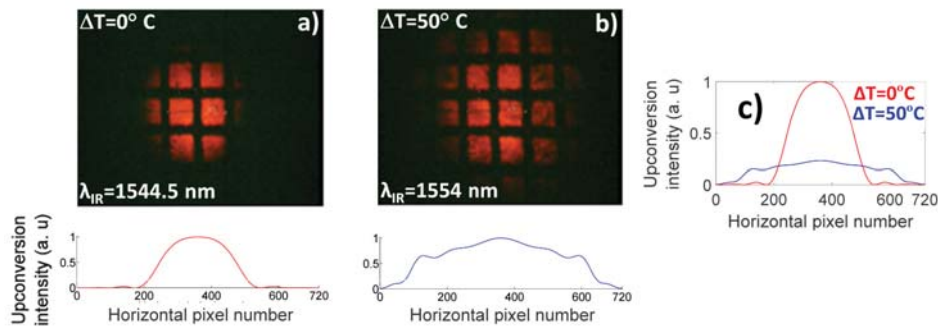


Fig. 10. Enhancement of the upconverted area of the IR illuminated object after the application of a temperature gradient to the PPLN.

In order to plot the application of a thermal gradient in the upconversion of IR images, we inserted a square pattern printed in a transparent film as the target for the IR illumination. We firstly illuminated the target with a $\lambda_{\text{IR}} = 1544.5\text{ nm}$ at room temperature and with no temperature gradient applied ($T = 22^\circ\text{C}$, $\Delta T = 0^\circ\text{C}$) and recorded the upconverted image [Fig. 10(a)]. This is the wavelength and temperature for perfect QPM in our PPLN crystal and

represents the case of nearly-collinear interaction. Secondly, we applied a temperature difference to the PPLN facets of $\Delta T = 50^\circ\text{C}$ ($T_{S1} \approx 75^\circ\text{C}$, $T_{S2} \approx 25^\circ\text{C}$) and tuned the IR illumination to $\lambda_{\text{IR}} = 1554\text{ nm}$ [Fig. 10(b)]. Under these conditions noncollinear upconversion is also enabled and the upconverted area is effectively increased exploiting single-wavelength illumination. In the lower part of Fig. 10, the calculated upconverted profile (in the absence of square patterns) including nonlinear temperature gradient and gaussian IR illumination is also provided for comparison. In [Fig. 10(c)] the angular distribution of the upconversion efficiency is presented relative to that of $\Delta T = 0^\circ\text{C}$.

It is also advantageous, from the point of view of image upconversion, not only to broaden the upconverter angular response but this to have a smooth variation or, equivalently, a low ripple with respect to the incoming IR angle. In this regard, wavelength allocation of the IR illumination is of importance. Upconverted profiles were recorded for $\Delta T = 30^\circ\text{C}$ at different IR illumination wavelengths (ranging from 1546 nm to 1560 nm in 2 nm steps) and compared with the calculated profiles making use of Eq. (5) and nonlinear thermal gradient at the same wavelengths. As it is depicted in Visualization 3, there is not a widening with smooth angular dependence for all IR illumination wavelengths and a given ΔT . From a certain point, by increasing the wavelength, an upconversion angular response which is no longer smooth with the IR incoming angle is achieved and it enhances more notably some angles in contrast to others. In addition, our calculations match well with measurements and, thus, can be of use in selecting the illumination wavelength for optimization of the upconverted area broadening in imaging applications.

In Fig. 11, we compare the field-of-view enhancement by two different techniques. The angular response of the crystal with no gradient and illuminated for perfect phase-matching ([Fig. 11(a)] shown as reference) is broadened by both illuminating with multiple-wavelengths (Amplified Spontaneous Emission, ASE, source) [Fig. 11(b)] and illuminating with a single-wavelength and a thermal gradient of $\Delta T = 40^\circ\text{C}$ [Fig. 11(c)]. As a proof of the coherence in the PPLN gradient upconversion process (due to single-wavelength illumination), we found interference fringes in the upconverted profiles as a consequence of the interference filters employed. For practical systems using this technique, it could be more suitable to employ dichroic filters instead.

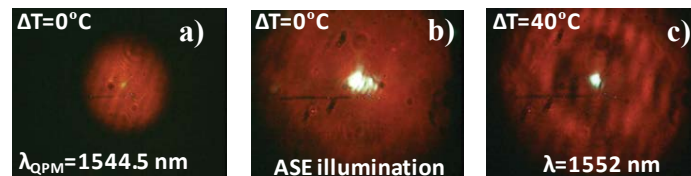


Fig. 11. Increased field-of-view if compared to a) upconverted profile at perfect QPM, b) for ASE illumination and c) after application of linear temperature gradient to the PPLN for single-wavelength illumination.

5. Conclusions

In this work we studied the increase of the upconverted area in an IR-to-visible image upconverter when a thermal gradient is applied through the nonlinear crystal. In particular we have studied angular response and image formation in short length PPLN crystals that are of interest in upconverters based on compact microchip laser, which might enable its widespread use. We have shown the feasibility of this technique for spreading the angular response of the upconverter under single-wavelength infrared illumination, in contrast to previous works where infrared illumination comprising several wavelengths was employed as a means of enhancing the upconverted area.

The upconverter angular response spreading is mainly influenced by the temperature difference between crystal edges. For a given temperature difference, both edges crystal

temperatures (T_{S1} and T_{S2}) and linearity of the gradient determine smoothness of the angular response for a given illumination IR wavelength. Therefore, for image upconversion applications, it becomes of importance to have a correct prediction of the upconverter angular response in order to widen the angular response while keeping a smooth angular response. We have compared calculated and measured upconverted profiles and found an adequate agreement between them. Although, as an alternative technique, angular broadening could be also expected from PPLN structures with a chirped poling period, angular enhancement by means of a thermal gradient may be preferred in terms of cost and reconfigurability of the upconverter. From the differences between calculations of $\eta'(\theta, \lambda_{IR})$ for both linear and nonlinear thermal distribution, future work could focus on engineering of the thermal distribution to conform a given angular response.

Funding

European Commission's FEDER (ERDF); Ministerio de Economía y Competitividad (Spain) under Project TEC2014-60084-R.